A95- 26665 AIAA-95-1292-CP

EULER/NAVIER-STOKES FLOW COMPUTATIONS ON FLEXIBLE CONFIGURATIONS FOR STABILITY ANALYSIS

Guru P. Guruswamy * and Eugene L. Tu**
Applied Computational Aerodynamics Branch, MS 258-1
NASA Ames Research Center, Moffett Field, California 94035-1000

Abstract

Longitudinal dynamic stability derivatives required for design of aircraft are computed by using the state-of-the-art numerical methods for wing-body configurations. The flow is modeled using the Euler/Navier-Stokes equations with turbulence models and solved using an efficient finite-difference scheme suitable for patched structured grids. Computations are made at a flow regime that is beyond the limits of the current linear methods mostly used for computing stability derivatives. Flow conditions include shock-waves and viscous dominated vortical flows. Effect of Mach number and angle-of-attack on stability derivatives are demonstrated for a typical wing-body configuration. For the same configuration the effects of wing flexibility on the magnitude and phase angles of stability derivatives are also demonstrated.

Introduction

Stability derivatives are required for design of aircraft. Most of the current stability derivative computations are based on the linear aerodynamic theory which is not adequate for transonic/vortical/separated flows where flows are dominated by strong nonlinearities, including moving shock waves. In addition to flow non-linearities, aircraft flexibility can significantly influence stability derivatives. Earlier wind tunnel measurements made on the Boeing 2707 SST model show significant differences in stability derivatives between rigid and flexible configurations.[1] Those differences are more pronounced in the transonic regime. Typical results in Ref. 1 show that the stability derivatives for the rigid and flexible configurations differ by as much as 30% at a transonic Mach number near 0.90.

In order to accurately determine stability derivatives associated with strong flow non-linearities, current practice is to conduct wind-tunnel tests. Wind-tunnel tests for transonic flows are not only expensive, but can also be time consuming. Furthermore, including important flexibility effects can make wind-tunnel experiments even more expensive and can often be more dangerous. As a result, parallel work using computational methods is required to confirm and complement wind tunnel measurements. Computational models are considerably less expensive and can yield early useful results which can help wind tunnel tests. With this effort, the overall cost of analysis and design of aircraft can be reduced considerably.

In order to accurately model non-linear flows that involve moving shock waves, vortices and flow separations, exact equations such as the Euler/Navier-Stokes equations are required. For the past two decades, Computational Fluid Dynamics (CFD) methods have made significant progress. Codes based on the Euler/Navier-Stokes equations coupled with structural equations are in routine use. At NASA Ames Research Center, significant effort has been made to develop a computer code, ENSAERO, that simultaneously solves the Euler/Navier-Stokes flow equations and modal/finite-element structural equations.[2] This code has been extended to compute unsteady flow on complex rigid configurations such as wing-body-canard and wing-body-control configurations by using patched zonal grids.[3,4] ENSAERO has a capability to compute aeroelasticity of wing-body configurations by using modal/finite-element structures with aeroelastically deforming built-in grids.[5]

In this work, the capability of ENSAERO to compute stability derivatives associated with complex flows is demonstrated for flexible configurations. Longitudinal dynamic stability derivatives required for design of aircraft are computed by using the state-of-the-art numerical methods for rigid and flexible wing-body configurations. Computations are made at a flow regime that is beyond the limits of the linear methods mostly used for computing the stability derivative. Flow conditions include shock-waves and viscous dominated vortical flows. Effect of Mach number and angle-of-attack on stability derivatives are demonstrated for a typical wing-body configuration. For the same configuration the effect of wing flexibility on the magnitude and phase angles of stability derivatives is also demonstrated.

* Research Scientist, AIAA Associate Fellow
** Research Scientist, AIAA Member

Governing Aerodynamic Equations

The strong conservation-law form of the Navier-Stokes equations are used for shock capturing purposes. The thin-layer version of the equations in generalized coordinates can be written as[6]

$$\partial_\tau \hat{Q} + \partial_\xi \hat{E} + \partial_\eta \hat{F} + \partial_\zeta \hat{G} = Re^{-1} \partial_\zeta \hat{S} \qquad (1)$$

where $\hat{Q}, \hat{E}, \hat{F}, \hat{G}$, and $\hat{S}$, are flux vectors in generalized coordinates. The following transformations are used in deriving Eq. (1).

$$\tau = t$$
$$\xi = \xi(x, y, z, t)$$
$$\eta = \eta(x, y, z, t)$$
$$\zeta = \zeta(x, y, z, t)$$

It should be emphasized that the thin-layer approximation is valid only for high Reynolds number flows and very large turbulent eddy viscosities invalidate the model.

To solve Eq. (1), ENSAERO has time-accurate methods based on central-difference method.[7]

Moving Grids for Flexible Configurations

One of the major difficulties in using the Navier-Stokes equations for computational aerodynamics lies in the area of grid generation. For steady flows, the advanced techniques such as zonal-grids are currently being used. However, grid-generation techniques for aeroelastic calculations, which involve moving components, are still in the early stages of development.

In this work, an H-O type grid topology is used. This grid topology is more suitable for general wing-body configuration. The base surface grid is generated using the S3D code.[8] From the surface grid, the flowfield grid is generated using the elliptic grid code 3DGRAPE.[9] For flexible configurations, the displacements at surface grid points are first computed. Then the flowfield grid is algebraically generated by redistributing the points along ζ grid lines that are in the radial direction starting normal to the surface. The grid points are redistributed by moving them along ζ grid lines. Each grid point is displaced by a value that is equal to the surface displacement times the arc length measured from the outer boundary. Thus the flowfield grid will match with the structural displacements at the surface and will also remain stationary at the outer boundary. This concept was utilized in Ref. 12 to quickly and efficiently generate the static grids at different canard deflections.

Results

Effect of Wing Flexibility on Time Responses

In this paper a typical wing-body configuration shown in Fig. 1 is selected for demonstration. For this rigid configuration, the measured aerodynamic and stability derivative data are given in Ref. 10 and 11. For this rigid configuration, steady, unsteady, and aeroelastic computations were made in Ref. 6 using ENSAERO.

In Ref. 6, the wing-body configuration shown in Fig. 1 was modeled using a H-O type grid and a grid refinement study was conducted. It was concluded that a grid size of 95 x 79 x 30 is adequate for computing pressures up to 12 deg angle of attack(AoA). The grid topology is shown in figure 1.

Steady state computations which are required as initial conditions for unsteady computations were made at several flow conditions and results are compared with the experiment. Typical computations required about 1000 steps for the residual to drop by three orders of magnitude. Figure 2 shows the comparison between the computed and the measured data at $M_\infty = 0.90$, $Re_c = 1.52$ x 10^6, and $\alpha = 4.09$ deg. The comparison is favorable. For this case, the flow is dominated by the presence of a moderate vortex and a weak shock-wave on the wing. This can be seen in the pressure-suction peaks near the leading edge in Fig. 2.

In order to study the effect of flexibility on aerodynamic force responses, computations are made on rigid and flexible configurations. In this paper, effect of wing flexibility in time responses are studied. Computations are made for 0 to 12 deg AoA at Mach numbers varying from 0.90 to 1.10 for rigid and flexible configurations in which the wing is oscillating in its first torsional mode. From the previous studies in Ref. 12, it was found that at these conditions the flow is dominated by leading edge vortices. For both rigid and flexible computations, the complete configuration was oscillating in the pitching mode with an amplitude of 1 deg about a pitch axes located at 2.45 root chords from the nose of the body. For the flexible case, the wing is oscillating in phase with the complete configuration with a tip amplitude of 1 deg. The reduced frequency, $k = \frac{\omega \bar{c}}{2U_\infty}$, is 0.5 for both configuration and wing oscillations.

At AoA = 0.0 computations were made using the Euler option of the code. The first grid spacing used is 0.005 of the root chord. The Euler computations required 2400 time steps per cycle. Two cycles were required during which the numerical transients disappeared and a periodic solution was obtained. The leading and trailing edge responses of the wing tip for the rigid and flexible configuration are shown in Fig. 3. The motion was started by first pitching downwards. As a result the tip is initially displaced upwards since

the axes of rotation for the configuration is forward of the wing-tip of leading edge.

Figures 4 and 5 show the effects of flexibility on total lift and moment responses, respectively, for M = 0.96. Both the lift and moment responses of the flexible case leads the rigid case in phase. The wing flexibility reduces magnitude of both the lift and moment. The flexible case has reduced the phase angle with respect to the motion when compared to the rigid case. Figures 6 and 7 show the effect of Mach number on magnitude and phase angles of lift for both rigid and flexible cases, respectively. For both cases the magnitude increases and the phase angle decreases with the increase in Mach number.

Computations similar to that carried out at AoA = 0 deg were also made at AoA = 4 deg by using the Navier-Stokes flow equations. A grid spacing of the order 0.00001 of root chord was used at the surface and the computations required 9000 time steps per cycle. Two cycles were required during which the numerical transients disappeared and a periodic solution was obtained. Figures 8 and 9 show the effect of flexibility on the magnitude and phase angles of the lift coefficient at various Mach Numbers ranging from 0.90 to 1.05. The magnitude of lift for both rigid and flexible cases decreases with the increase in Mach number. The magnitude of lift for the flexible case is always lower than that of the rigid case. Both phase angles in Fig. 9 increase with the increase in Mach number. This is opposite to what was observed at AoA = 0 deg. The flexible case again leads the rigid case for all Mach numbers, similar to the case of AoA = 0 deg.

It was also of interest to study the effect of angle of attack on force responses. Computations were made at 0, 4, 8 and 12 deg mean AoA. Figures 10 and 11 show the effect of AoA on magnitude and phase angles for both rigid and flexible cases, respectively. Lifts for both rigid and flexible cases increase until about 4 deg AoA and start decreasing. At all AoA, the rigid cases have higher magnitudes than the flexible cases. The difference between rigid and flexible cases decreases slightly with the increase in AoA. Figure 11 shows that phase angles of the rigid cases increase until AoA of about 4 deg and then start decreasing. For the flexible case the phase angle continuously decreases and the rate of decrease slightly increases after 4 deg AoA. Again the phase angle behaviors are influenced by vortical flows.

The effect flexibility at various Mach numbers and AoA on the stability derivatives is studied in next section.

Effect of Wing Flexibility on Dynamic Stability

The dynamic stability parameters for the rigid and flexible wing-body configurations are predicted from the Fourier analysis presented in Ref. 3 of the computed normal force and pitching moment coefficients. Such an analysis yields Fourier coefficients that are directly related to the normal force and moment stability parameters given by $(C_{N_\alpha} - k^2 C_{N_{\dot{q}}})$, $(C_{N_{\dot{\alpha}}} + C_{N_q})$, $(C_{m_\alpha} - k^2 C_{m_{\dot{q}}})$, and $(C_{m_{\dot{\alpha}}} + C_{m_q})$. The first two terms represent pitch displacement and pitch rate parameters while the last two terms represent oscillatory stability and damping-in-pitch. Further details of predicting dynamic stability parameters are given in Ref. 3.

In the current study, the effects of flexibility on dynamic stability parameters for the wing-body configuration are examined. To validate the techniques presented in this study, a comparison with experimentally measured dynamic stability parameters for the rigid configuration is given in Fig. 12. In order to match with experimental flow conditions, the computations are performed at a freestream Mach number of 0.70 and a pitch amplitude of 1 deg. In Fig. 12, stability parameters based on normal force coefficients are given for oscillations about various mean angles of attack.

The effect of flexibility on dynamic stability parameters at various Mach numbers are given in Fig. 13 for mean AOA of 4 deg. Figures 13a-13d represent pitch rate, pitch displacement, damping-in-pitch and oscillatory stability parameters, respectively, as defined above. It is noted from Fig. 13 that the effects of flexibility are most pronounced in the pitch displacement and oscillatory stability parameters for the entire Mach number range. In fact, the effect of in-phase wing flexibility as defined in this study leads to a decrease in positive oscillatory stability ($(C_{m_\alpha} - k^2 C_{m_{\dot{q}}}) < 0$). Figure 13 also shows that more significant changes in stability parameters as a function of Mach number occur in the transonic regime of M = 0.90 to 1.0.

Figure 14 illustrates the effect of AoA on dynamic stability parameters at a Mach number of 0.95. As in Figure 13, more pronounced changes between rigid and flexible cases are noted for the pitch displacement and oscillatory stability parameters. As in the earlier phase and magnitude results, significant non-linear responses are noted throughout the angle of attack range.

Conclusions

The use of the Euler/Navier-Stokes flow equations to compute stability parameters required for design are demonstrated. Computations are made at transonic/vortical flow conditions which are beyond the limits of current codes based on the linear aerodynamic theory typically used in stability parameter computations. Capability of current high fidelity based flow codes to account for flexibility is also demonstrated.

Computations are made for transonic/vortical flows at various Mach numbers and angles of attack for

both rigid and flexible cases. It is found that for the configuration selected with a highly swept wing, the flow characteristics were moderately non-linear with respect to Mach number and angle of attack. Even at these moderate non-linear flow conditions, the wing flexibility influenced the responses and stability parameters considerably.

Though this work demonstrated the feasibility of using the Euler/Navier-Stokes equations for computing the stability parameters, the associated computational expense is still an issue. Order of magnitude speed-up is required to make this a routine design tool. Such speed-up can be achieved by using the advanced computing systems such as parallel computers.

References

[1] Anon., "An Analysis of Methods for Predicting the Stability Characteristics of Elastic Airplanes," NASA CR-73275, Nov 1968.

[2] Guruswamy, G.P., "ENSAERO - A Multidisciplinary Program for Fluid/Structural Interaction Studies of Aerospace Vehicles," Computing Systems Engineering, Vol. 1, Nos. 2-4, 1990, pp237-256.

[3] Tu, E. L., "Navier-Stokes Simulation of the Canard-Wing-Body Longitudinal Dynamic Stability Characteristics," AIAA-94-1901, 12th Applied Aerodynamics Conference, Colorado Springs, June 20-23, 1994.

[4] Obayashi, S., Chiu, I., and Guruswamy, G. P. "Navier-Stokes Computations on Full-Span Wing-Body Configuration with Oscillating Control Surfaces," AIAA-93-3687, AIAA Atmospheric Flight Mechanics Conference, Monterey, August 9-11, 1993.

[5] Guruswamy, G.P. and Byun, C., "Fluid-Structural Interactions Using Navier-Stokes Flow Equations Coupled with Finite Element Structures," AIAA-93-3087, 24th Fluid Dynamics Conference, Orlando FL, July 6-9, 1993.

[6] Peyret, R. and Viviand, H., "Computation of Viscous Compressible Flows Based on Navier-Stokes Equations," AGARD AG-212, 1975.

[7] Beam, R. and Warming, R.F., "An Implicit Finite-Difference Algorithm for Hyperbolic Systems in Conservation Law Form," **J. of Comp. Phys.**, Vol. 22, No. 9, Sept. 1976, pp. 87-110.

[8] Luh, R. C., Pierce, L. and Yip, D., "Interactive Surface Grid Generation," AIAA Paper 91-0796, Reno Nevada, Jan 1991.

[9] Sorenson, R. L., "The 3DGRAPE Book: Theory, Users' Manual, Examples, " NASA TM 102224, July 1989.

[10] Gloss, B. B. ,"Effect of Canard Location and Size on Canard-Wing Interference and Aerodynamic-Center Shift Related Maneuvering Aircraft at Transonic Speeds," NASA TN D-7505, June 1974.

[11] Gloss, B.B, "Effect of Canard Location and Size on Canard-Wing Interference and Aerodynamic-Center Shift Related to Maneuvering Aircraft at Transonic Sppeds," NASA TN D-7505, June 1974.

[12] Tu, E. L., " Effect of Canard Deflection on Close-Coupled Canard-Wing-Body Aerodynamics," AIAA 92-2602, Palo Alto California, June 1992.

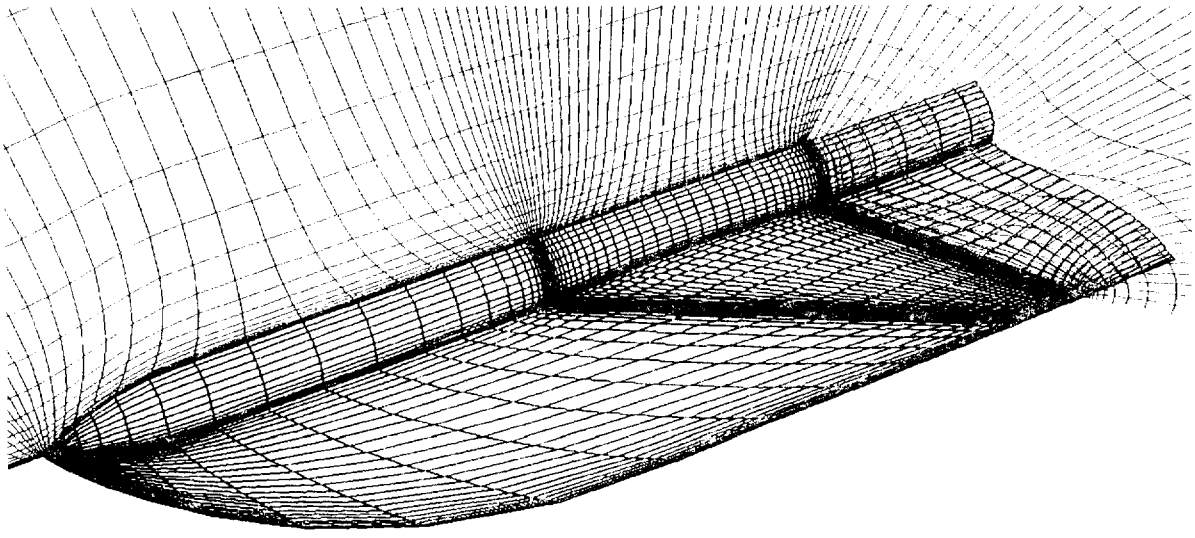

Fig. 1 The grid topology of the wing-body configuration.

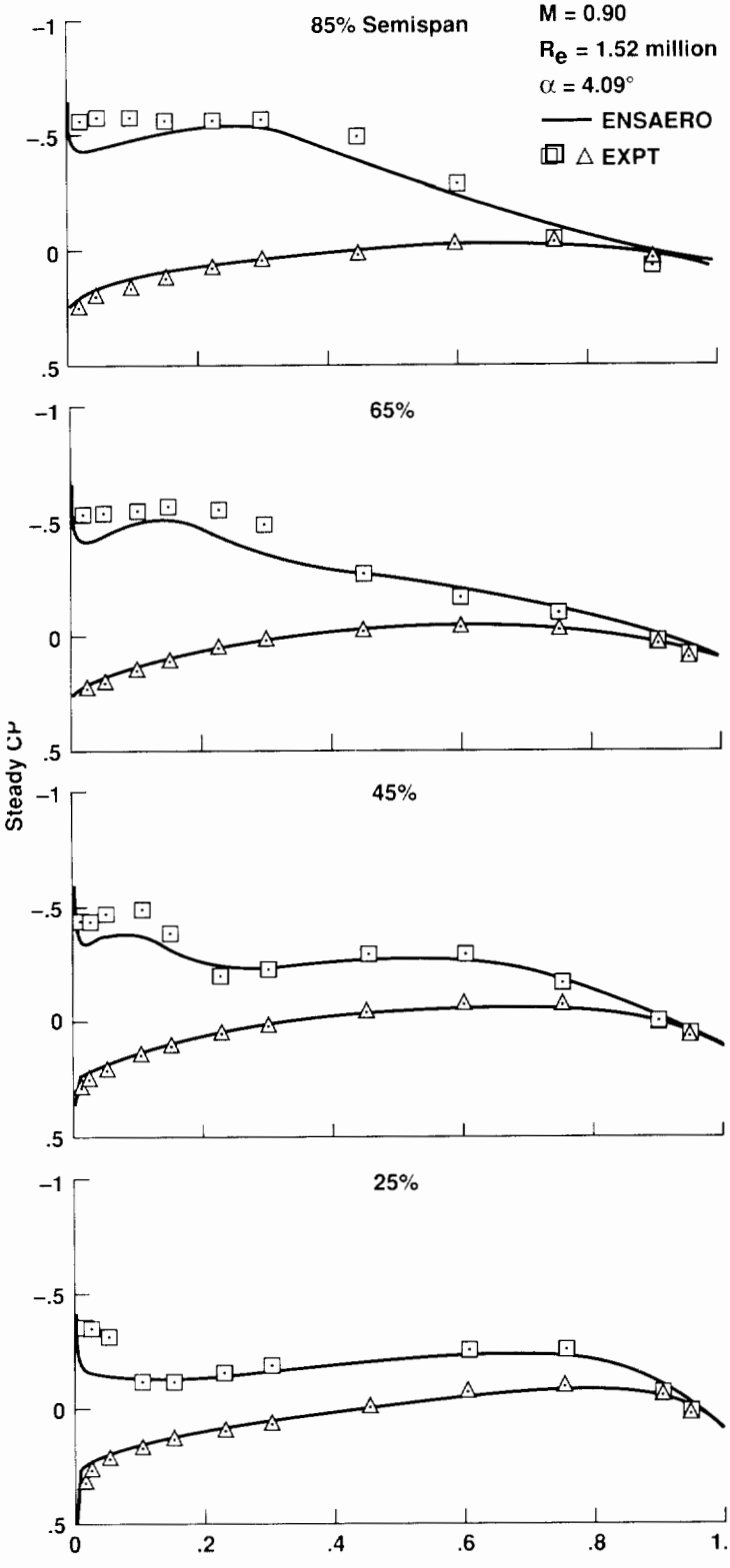

Fig. 2 Comparison between computed and measured pressure distributions at M = 0.90 and α = 4.09 deg

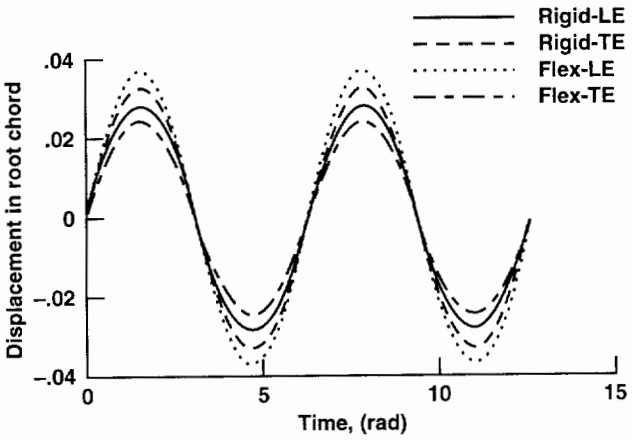

Fig. 3 Comparison of displacements at wing tip between rigid and flexible cases

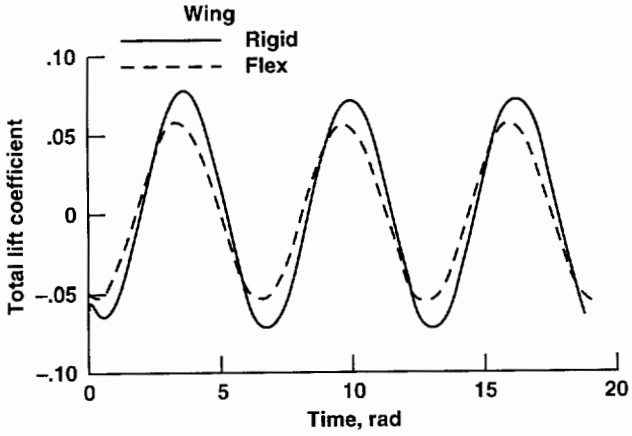

Fig. 4 Comparison of total lift responses between rigid and flexible cases at M = 0.95, α = 0 deg and k = 1.

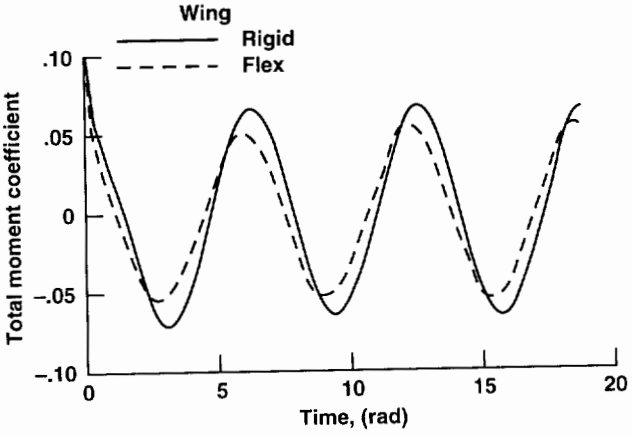

Fig. 5 Comparison of moment responses between rigid and flexible cases at M = 0.95, α = 0 deg and k = 1.

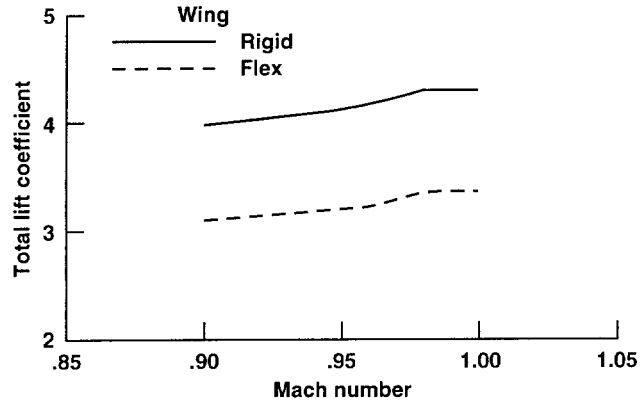

Fig. 6 Effect of Mach number on the magnitude of lift for rigid and flexible cases at $\alpha = 0$ deg and k = 1.

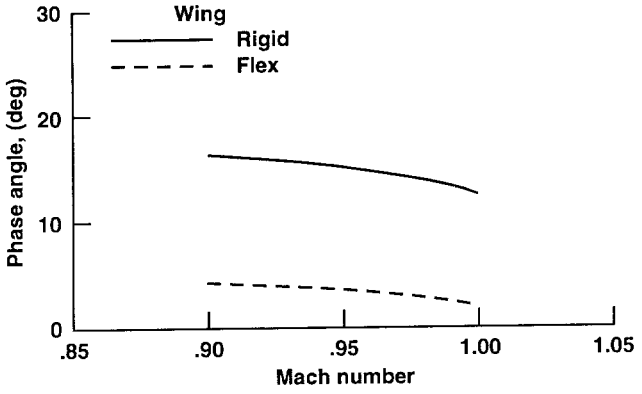

Fig. 7 Effect of Mach number on the phase angle of lift for rigid and flexible cases at $\alpha = 0$ deg and k =1.

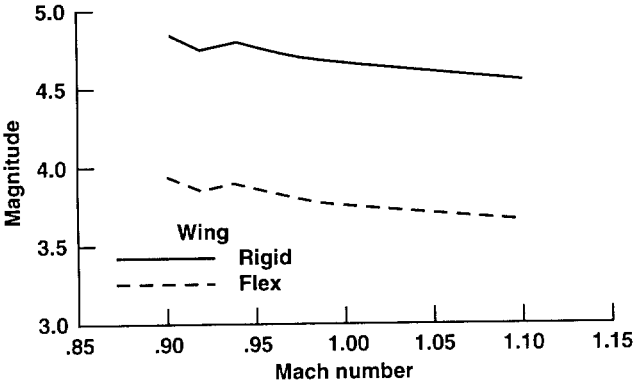

Fig. 8 Effect of Mach number on the magnitude of lift for rigid and flexible cases at $\alpha = 4$ deg and k = 1.

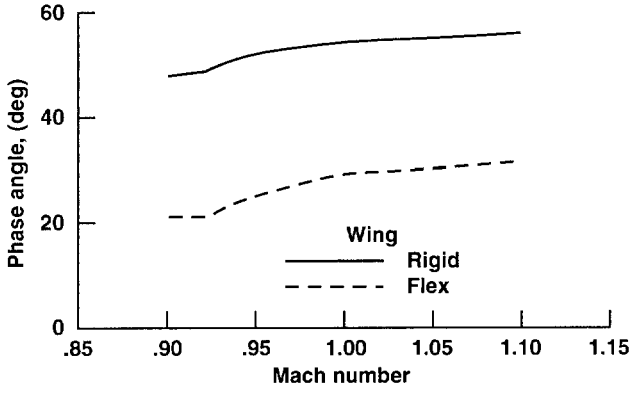

Fig. 9 Effect of Mach number on the phase angle of lift for rigid and flexible cases at $\alpha = 4$ deg and k =1.

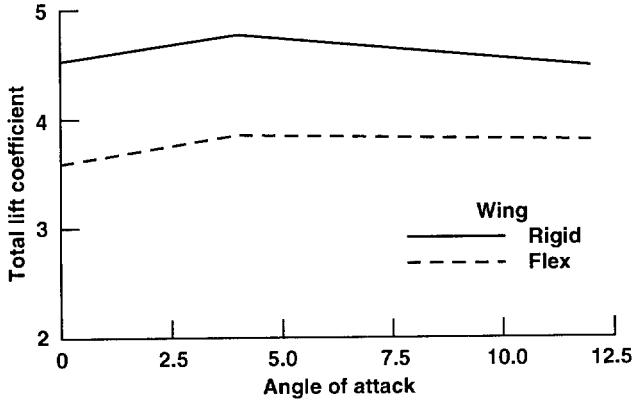

Fig. 10 Effect of angle of attack on the magnitude of lift for rigid and flexible cases at M = 0.95 and k = 1.

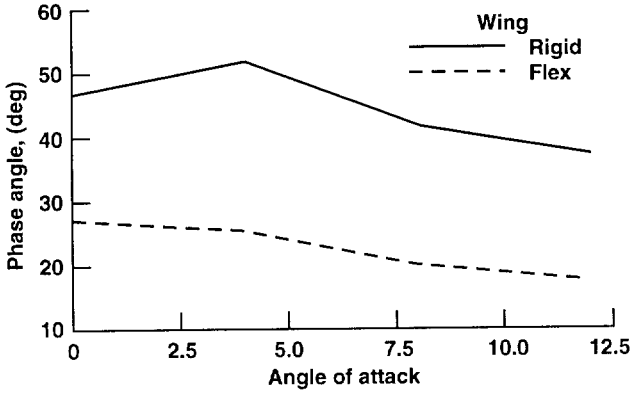

Fig. 11 Effect of angle of attack on the phase angle of lift for rigid and flexible cases at M = 0.95 and k =1.

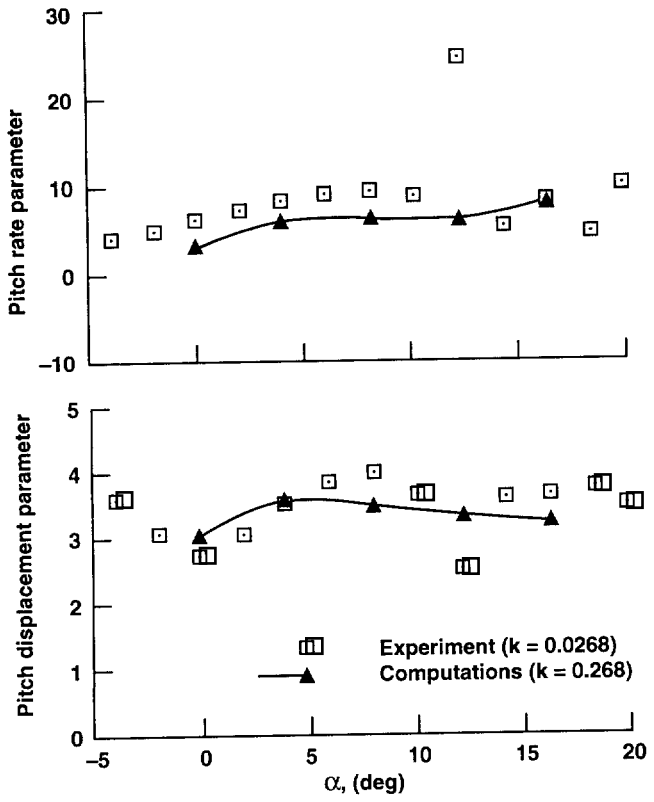

Fig. 12 Comparison of pitch rate and pitch displacement stability parameters between computations and experiment at various angles of attack for M = 0.70 and k = 0.268.

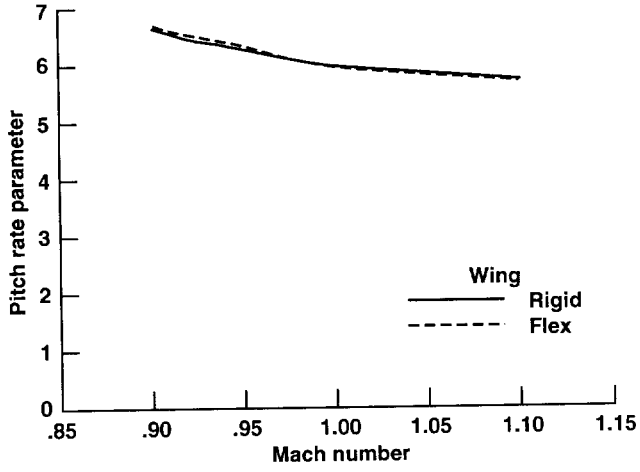

Fig. 13-a Effect of Mach number on rigid and flexible pitch rate parameter for cases at α = 4 deg and k = 1.0.

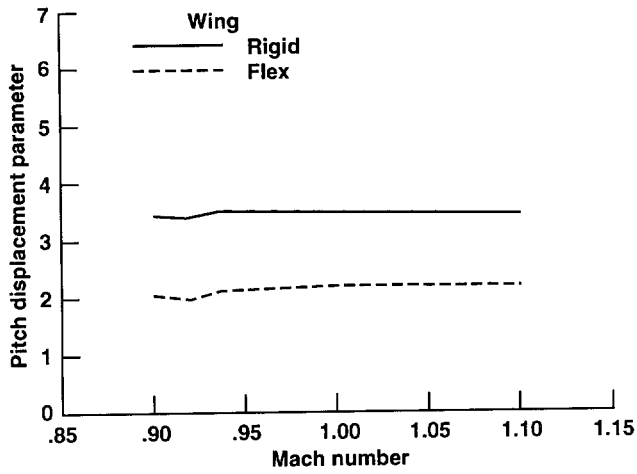

Fig. 13-b Effect of Mach number on rigid and flexible pitch displacement parameter at α = 4 deg and k =

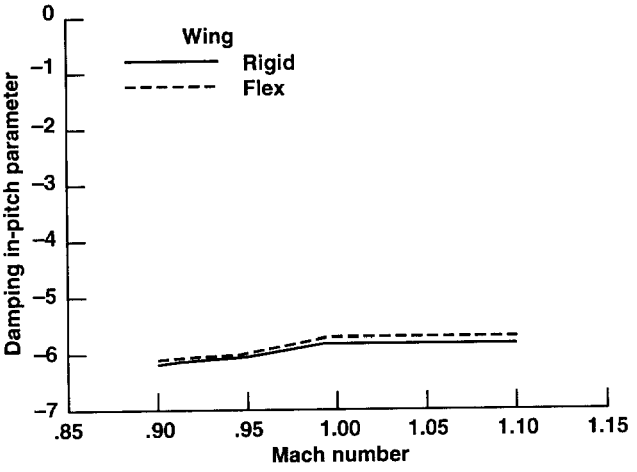

Fig. 13-c Effect of Mach number on rigid and flexible damping-in-pitch parameter at α = 4 deg and k = 1.0.

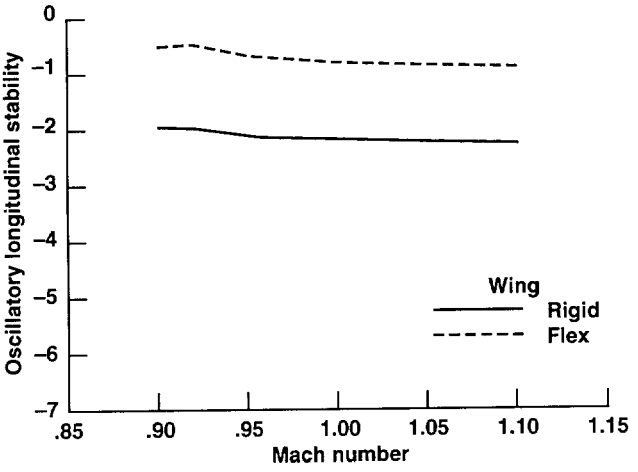

Fig. 13-d Effect of Mach number on rigid and flexible oscillatory longitudinal stability parameter at α = 4 deg and k = 1.0.

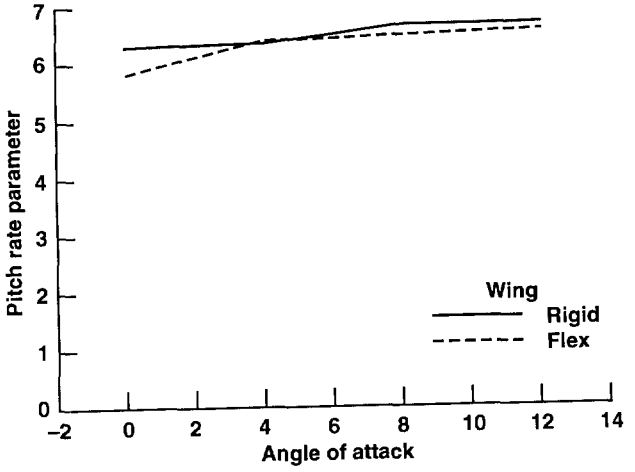

Fig. 14-a Effect of angle of attack on rigid and flexible pitch rate parameter at M = 0.95 and k = 1.0.

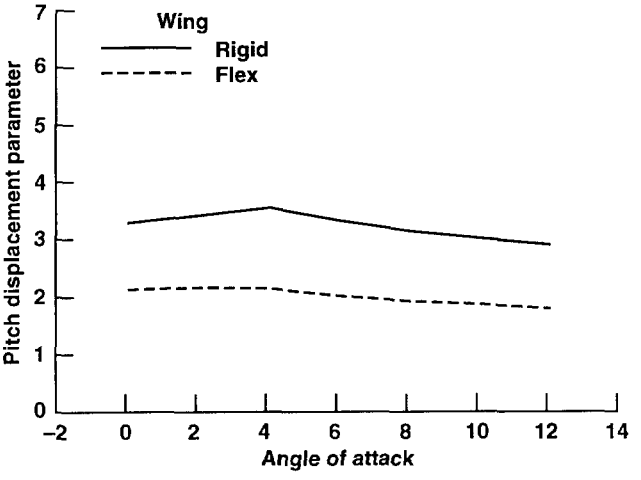

Fig. 14-b Effect of angle of attack on rigid and flexible pitch displacement parameter at M = 0.95 and k = 1.0.

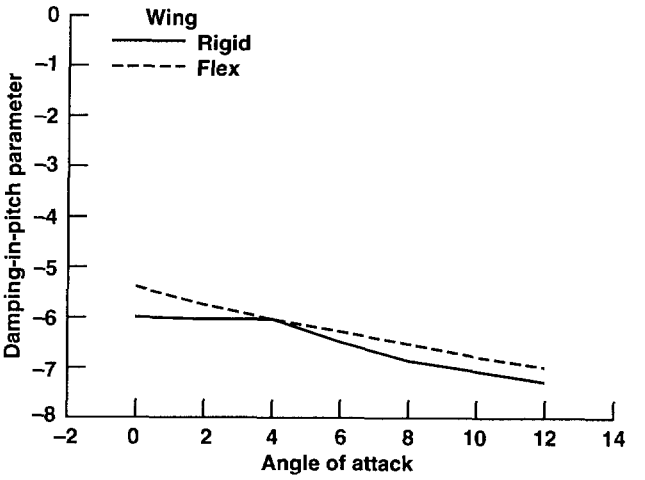

Fig. 14-c Effect of angle of attack on rigid and flexible damping-in pitch parameter at M = 0.95 and k = 1.0.

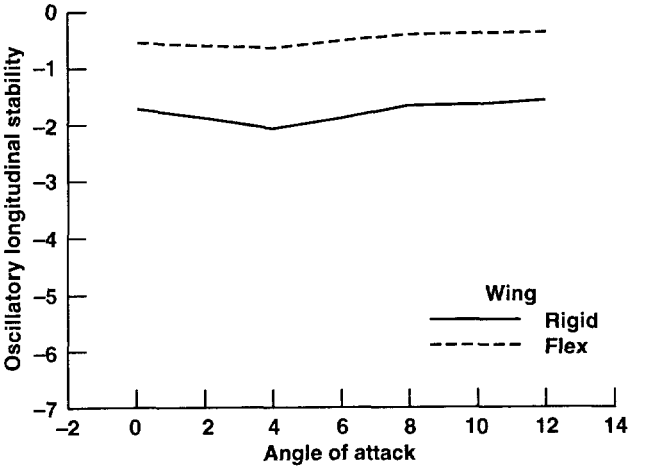

Fig. 14-d Effect of angle of attack on rigid and flexible oscillatory longitudinal stability parameter at M = 0.95 and k = 1.0.